ACS OMEGA

Open Access



http://pubs.acs.org/journal/acsodf

Article

# Crystallization Regulation Determined Spinnability and Mechanical Properties toward PA66/Calcium Chloride and Its Fibers

Jianing Wang, Jing Zhang, Yanlong Zhu, Shuo Yang, Zhenfeng Dong, Xiuqin Zhang,* and Rui Wang

Cite This: *ACS Omega* 2025, 10, 19444−19452

Read Online

ACCESS | Metrics & More | Article Recommendations | Supporting Information

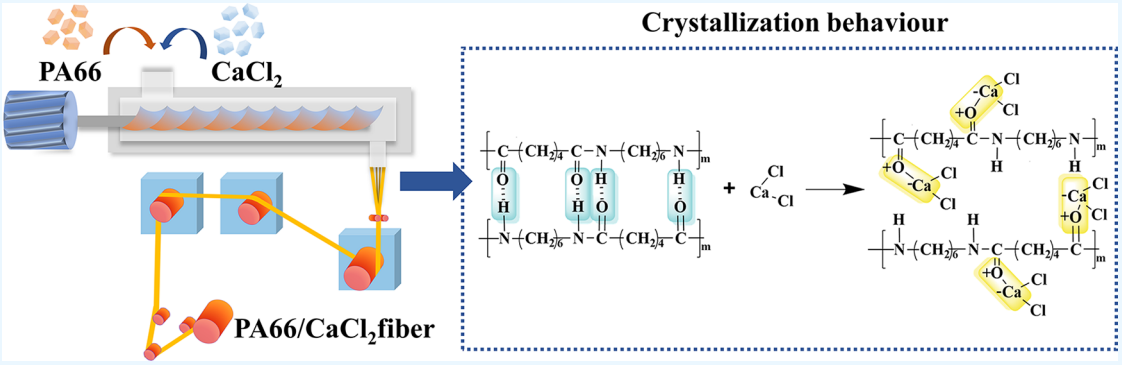


**ABSTRACT:** Strong hydrogen bonding and the fast crystallization rate of polyamide 66 (PA66) bring difficulties in the fabrication of high-performance PA66 fibers. In this work, calcium chloride ($CaCl_2$) was used as a modifier to regulate the crystallization rate and drawing performance of PA66. With the increased presence of $CaCl_2$, the viscosity of PA66/$CaCl_2$ increased, and the crystallization rate was significantly suppressed. At 5 wt % $CaCl_2$, the crystallinity decreased from 31.36 to 19.52%, indicating a notable inhibition effect. The isothermal FTIR mechanism studies elucidated that a blueshift of the N−H stretching vibration can be observed, which resulted from the complexation between $Ca^{2+}$ and the oxygen atoms on the amide groups disrupting the original hydrogen bond. The inhibition of hydrogen bonds promotes the fabrication of PA66 fiber with a draw ratio at 3.5 and a breaking strength at 5.16 cN/dtex. This work provides an effective way to enhance the spinnability and drawability of PA66 fibers.

## 1. INTRODUCTION

Polyamide 66 (PA66), also known as nylon 66, is a thermoplastic textile material, which is widely applied in the textile field due to its excellent performance such as high strength, excellent elasticity, abrasion resistance, fatigue resistance properties, etc.[1−5] The amine groups as the repeating unit on the main chain of PA66 possess abundant hydrogen bonds, which promotes the formation of complex crystals and thus endows the PA66 with excellent comprehensive performance.[6,7] However, the rapid crystallization rate resulting from the hydrogen bonds also restricted the tensile deformation behavior, high draw ratio, and ideal mechanical property for PA66 fiber. Researchers have carried out different methods to produce high-modulus fiber such as solution spinning, dry spinning, wet spinning, gel spinning, and zone drawing and annealing.[8−10] It is reported that the suppression of crystallinity and modification of the number and strength of the hydrogen bonds within the polymer crystals are effective methods to achieve a high draw ratio through tensile drawing.

The application of complexing agents, such as iodine, anhydrous ammonia, metal salt, and rare-earth materials, is reported to weaken intermolecular interactions, improve tensile properties, and thus obtain the high-strength and high-modulus fiber.[11−14] Among those materials mentioned above, metal salts are the promising materials that showed satisfactory modification performance and did not possess a poisonous component. For example, Ciferri et al. reported that LiCl and LiBr could significantly reduce the crystallization rate of PA.[15] The Young's modulus of the PA6/lithium halide fibers can be improved significantly via drawing and annealing.[16,17] Acierno et al.[18,19] reported that with the addition of 2 wt % LiCl, the melting point of PA6 decreased by 15 °C. Rare-earth ions also manifest a strong coordination ability to amide groups. The coordination effect between polyamine and rare-earth metal salts ($GaCl_3$) was reported to completely disrupt the hydrogen intermolecular bonds. The strong coordination bonds in the yttrium-containing PA6 composites change the hydrogen bonds,[20] which is verified by the appearance of new

Received: December 5, 2024
Revised: April 17, 2025
Accepted: April 22, 2025
Published: May 8, 2025

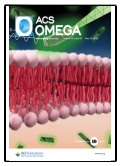

bands in the amide A and amide I regions in FTIR and Raman spectra. Moreover, it has been found that the lanthanide complexes helped improve the spinnability of PA6 fibers. As a result, fine denier PA6 fibers were successfully prepared. With similar mode of interaction to calcium chloride ($CaCl_2$), the $CaCl_2$ solution is reported to improve the interfacial adhesion of PA66 via complexation interactions.[21−23] In the $CaCl_2$/formic acid/$CHCl_3$ dry spinning process, the high-performance PA6 fiber with a strength at 0.66 GPa can be achieved via complexation.[24]

The fundamental studies on the crystallization behavior of polyamine would further guide the manufacturing parameters of PA66 fiber.[25−28] For example, Zhang et al.[29] reported that the $\beta$ phase crystal can be obtained in PA6 fibers when the melt draw ratio is relatively high, while the $\gamma$ phase crystal predominated when the melt draw ratio was relatively low. The $\beta$ phase may act as an intermediate state upon the phase transformation from $\gamma$ to $\alpha$ occurring during a drawing process. Zhang et al. studied the differences between the bimodal crystallization kinetics of PA66 and PA6. Both PA66 and PA6 exhibited a bimodal kinetics profile with crystallization rate minima at 135 and 110 °C, respectively.[30] The kinetic profile indicated that PA66 crystallizes even faster than PA6 regardless of the polymorphs formed. Moreover, due to the stronger hydrogen bonding of PA66 than PA6, the stress-induced crystallization at room temperature did not occur. However, a rapid transformation from a hedrite morphology to a fibrillar one was observed.[31] Due to the faster crystallization rate and higher processing temperature, limited work reported the crystallization behavior of PA66. However, the above-mentioned crystallization regulation toward PA6 fiber would provide guidance for the preparation of PA66 fiber due to the similar amide groups between PA6 and PA66. Therefore, the investigation and regulation of the rapid crystallization behavior of PA66 are crucial to improve its spinnability and mechanical property.

In this work, $CaCl_2$ was applied as a modifier to regulate the crystallization behavior of PA66. PA66 composites containing a series of different loaded $CaCl_2$ were fabricated via melt blending. The effect of $CaCl_2$ on the structure and mechanical properties of PA66 was systematically studied. Finally, the PA66 fiber with an enhanced mechanical property was fabricated.

## 2. EXPERIMENTAL SECTION

**2.1. Materials.** Polyamide 66 was purchased from the China Shenma Group Co., Ltd. Calcium chloride was purchased from China Alfa Aesar Chemical Co., Ltd.

**2.2. Preparation of PA66/$CaCl_2$ Composites.** PA66 pellets and $CaCl_2$ powder were first dried at 120 °C for 12 h in a DZF-6050 vacuum oven (Shanghai Yiheng Technology Co., Ltd.). Then, PA66 composites with 1, 3, 5, and 8 wt % $CaCl_2$ were prepared by melt compounding in a Haake Rheomex OS twin-screw extruder (Thermo Fisher). The temperatures of the first to sixth zones of the screws were 280, 290, 290, 290, 290, and 280 °C, respectively, and the screw speed was 50 r/min. The obtained blends were named B0, B1, B3, B5, and B8 (Table 1).

**2.3. Preparation of PA66/$CaCl_2$ Fiber.** Pure PA66 pellets and PA66/$CaCl_2$ masterbatch with 8 wt % $CaCl_2$ addition were first dried in a DZF-6050 vacuum oven (Shanghai Yiheng Technology Co. Ltd.) at 120 °C for 12 h. Subsequently, PA66 and PA66/$CaCl_2$ nascent fibers were spun by an SJ-120 melt spinning machine (Dalian Hualun Chemical Fiber Equipment Co., Ltd.) with mass fractions of $CaCl_2$ at 0.5, 1, and 3% (named B0-F, B0.5-F, B1-F, and B3-F). The temperatures of the first, second, third, and fourth zones of the screw were 250, 275, 279, and 280 °C, respectively. The melt pipe temperature was 290 °C, and the spinning component temperature was 295 °C. The spinneret aperture was 0.25 mm and had 48 holes; the screw diameter was 25 mm, the ratio of length to diameter was 25, and the rotation speed was 20 r/min. The metering pump specification was 1.2 mL/r, and the rotation speed was 12 r/min. The winding speed of the nascent fiber was 1000 m/min. Then, the upper hot roller, lower hot roller, and thermal chamber temperatures of the drawing machine were set to 35, 30, and 145 °C, respectively, and the nascent fibers of PA66/$CaCl_2$ with 1 wt % $CaCl_2$ were subjected to hot drawing and the drawn fibers were named B1-F'.

Table 1. Composition of PA66/$CaCl_2$ Composites

| samples | PA66 (wt %) | $CaCl_2$ (wt %) |
|---|---|---|
| B0 | 100 | 0 |
| B1 | 99 | 1 |
| B3 | 97 | 3 |
| B5 | 95 | 5 |
| B8 | 92 | 8 |

**2.4. Characterizations.** Thermo gravimetric analysis (TGA) was conducted by a TGA8000 thermogravimetric analyzer (Seiko, Japan) at a temperature range of 30−600 °C in a $N_2$ atmosphere with a heating rate of 10 °C/min. Crystallization behaviors were characterized on a Q2000 (TA, USA) differential scanning calorimeter. For nonisothermal crystallization, the temperature was increased to 300 °C at 20 °C/min and kept constant for 3 min; then, the temperature was decreased to 20 °C at 10 °C/min and kept constant for 3 min; finally, the temperature was increased to 300 °C at 10 °C/min. The crystallinity of the polymers was calculated using eq 1 below, where $X_c$ is the crystallinity of the sample (%); $\Delta H_{cc}$ for the enthalpy of cold crystallization, J $g^{-1}$; $\Delta H_m$ for the thermal enthalpy value required for sample melting, J $g^{-1}$; $\Delta H_c$ for the thermal enthalpy value released during cold crystallization, J $g^{-1}$; $\Delta H_m^0$ for PA66 100% crystallization, 188.4 J $g^{-1}$.[32] The crystallinity is calculated as below:[33]

$$X_c\ (\%) = \frac{\Delta H_m - \Delta H_{cc}}{\Delta H_m^0} \quad (1)$$

For isothermal crystallization, the temperature was increased to 300 °C at 50 °C/min and maintained at a constant temperature for 3 min, then cooled down to the isothermal temperature at 50 °C/min, and maintained at a constant temperature for 20 min; in order to explore the melting point of the crystals of different samples crystallized isothermally, the temperature was increased to 300 °C directly from the isothermal crystallization temperature at 10 °C/min. Isothermal FTIR spectra of the samples were recorded on a Nicolet Nexus 670 Fourier transform infrared spectrometer (Thermo Nicolet Instruments, USA). The ATR mode was selected to test the wavenumber range from 4000 to 400 $cm^{-1}$ with 32 scans. For in situ infrared spectroscopy tests, a Nicolet 6700 Fourier transform infrared spectrometer (Thermo Fisher Scientific, USA) was used, and the detector was an MCT detector. The transmission mode was selected for the test with a spectral resolution of 1 $cm^{-1}$ and 16 scans in the wavelength


https://doi.org/10.1021/acsomega.4c11028
ACS Omega 2025, 10, 19444−19452

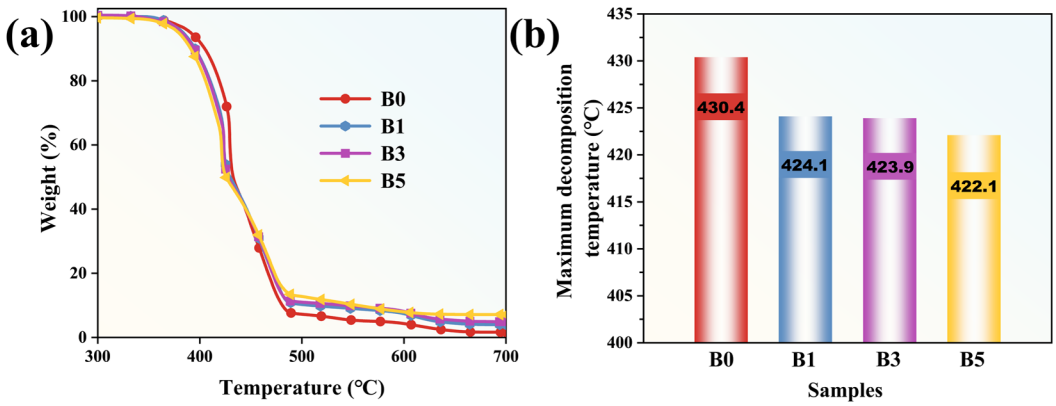


**Figure 1.** TGA curves (a) and maximum decomposition temperature (b) of PA66/$CaCl_2$ composites.

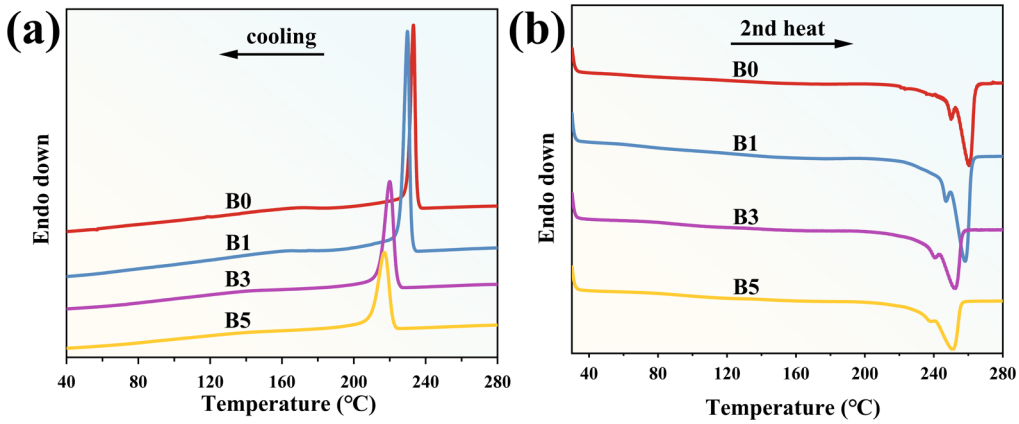


**Figure 2.** DSC scans of cooling curves (a) and heating curves (b) of PA66/$CaCl_2$ composites.

range of 4000−650 $cm^{-1}$. The samples were sandwiched between two potassium bromide salt tablets and placed on a hot bench. The samples were heated from room temperature to 250 °C at a rate of 10 °C/min, and spectra were collected at 30 s intervals. An Olympus BX51 polarizing microscope (Olympus Co., Ltd., China) coupled with a Linkam LT350 tensile hot stage (Linkman Scientific Instruments, UK) was used to test the spherical crystalline morphology change of PA66/$CaCl_2$ blends during the isothermal process of PA66 at 250 °C. The samples were placed in the middle of two circular glass sheets, melted at 300 °C to eliminate thermal history, and then rapidly cooled down to 250 °C at 50 °C/min and isothermal for 30 min to observe the crystallization process of the samples and collect pictures. Wide-angle X-ray scattering (WAXS) data were collected in a digital form from the films using a D8 DISCOVER-type 2D wide-angle X-ray diffractometer (BRUKER, Germany) operated at 40 kV and 20 mA with a Cu K$\alpha$ ($\lambda$ = 1.54 Å) radiation source. The treatment time was 180 s. WAXS data were collected on films. The signals were collected by a two-dimensional surface detector with a spacing of 85.6 mm between the detector and the sample. The obtained two-dimensional image was transformed into a one-dimensional curve by integrating along the azimuthal angle of 0−360° after subtracting the effect of background air scattering. The one-dimensional intensity profiles were subsequently peak-fitted, and the crystallinity ($X_c$) of PA66 was calculated as in eq 2, where $A_c$ and $A_a$ represent the area of crystalline and amorphous regions, respectively.[34]

$$X_c\ (\%) = \frac{A_c}{(A_c + A_a)} \times 100\ (\%) \tag{2}$$

The orientation factor of the crystalline structure was further evaluated using the Hermans orientation factor ($f$), as defined in eq 3, where $\varphi$ is the azimuthal angle and $\varphi$ = 0 corresponds to the fiber-axis direction. $\varphi$ was taken as the full width at half-maximum of the azimuthal distribution of intensity. In cases where the crystallites are isotropically distributed, $f$ = 0; when they are perfectly aligned along the flow direction, $f$ = 1.

$$f = \frac{3 < \cos^2\Phi > -1}{2} \tag{3}$$

A Rheomix 600P capillary rheometer (HAAKE, Germany) was used with a cylinder temperature of 280 °C, capillary $L/D$ = 36, $D$ = 1 mm, shear rate of 0−10,000 $s^{-1}$, and a preheating time of 5 min. A YG086C-type wisp yarn length gauge (Changzhou Second Textile Machinery Factory) was used to test the denier, and the PA66/$CaCl_2$ comeningled fibers were coiled for 100 laps of 1 m each. Each sample was repeated five times, and the average value was taken, weighed, and multiplied by 100 to get the fiber length of a bundle of fibers in dtex. An HD021NS single-yarn tester (Jiangsu Nantong Hongda Experimental Instrument Co., Ltd.) was used to perform fixed-speed tensile tests on PA66/$CaCl_2$ blended fibers with a clamping distance of 100 mm and a fiber tensile speed of 500 mm/min. The measurements of each sample were repeated five times, and the average values were taken to obtain the fiber breaking strength and elongation at break.


https://doi.org/10.1021/acsomega.4c11028
ACS Omega 2025, 10, 19444−19452

## 3. RESULTS AND DISCUSSION

**3.1. Thermal Properties of PA66 Composites.** The high melting temperature of PA66 is required for the high processing temperature in the melt blending, which was as high as 290 °C. Therefore, the thermal stability of the PA66 and the additive fillers is crucial to maintain its high performance. The thermogravimetric curves and the temperatures corresponding to the maximum decomposition rate of PA66/$CaCl_2$ blends in different proportions are shown in Figure 1. It can be observed that the initial decomposition temperature ($T_{5\%}$) of pure PA66 was 391.1 °C and the maximum decomposition temperature was at 430.4 °C. With the addition of $CaCl_2$, the maximum decomposition temperatures of B1, B3, and B5 gradually decrease to 424.1, 423.9, and 422.1 °C, respectively. In practical processing applications, the processing temperature of PA66 is around 290 °C; therefore, the addition of $CaCl_2$ has little effect on the melting and processing of PA66.

The DSC curves of PA66/$CaCl_2$ blends in different proportions are shown in Figure 2, and the corresponding thermal performance parameters are listed in Table 2. From Figure 2a, it can be seen that all samples exhibit a distinct single crystallization peak. As the mass fraction of $CaCl_2$ increases, the crystallization temperature gradually decreases. When the $CaCl_2$ content is 5 wt %, the crystallization temperature of the PA66/$CaCl_2$ blend decreases from 233.2 °C for pure PA66 to 217.0 °C. This indicates that the addition of $CaCl_2$ reduces the crystallization rate of PA66. This result is further confirmed by the second heating DSC curve of the blends. As shown in Figure 2b, with the increase in $CaCl_2$ content, the melting temperatures of the PA66/$CaCl_2$ blends are 260.4, 258.2, 252.6, and 251.1 °C, indicating that the addition of $CaCl_2$ reduces the perfection of PA66 crystals. Moreover, the crystallinity of PA66 blends modified with $CaCl_2$ decreases, and as the $CaCl_2$ content increases, the crystallinity of the blends further declines. When the $CaCl_2$ content is 5 wt %, the crystallinity of sample B5 drops from 40.4% for pure PA66 to 30.8% (Table 2), suggesting that the addition of $CaCl_2$ significantly inhibits the crystallization of PA66. This may be due to the coordination interaction between calcium ions in $CaCl_2$ and amide groups, which affects the hydrogen bonding in the PA66 system, thereby reducing the crystallization rate during heating and cooling.

To further investigate the effect of $CaCl_2$ on the crystallization behavior of PA66, isothermal crystallization tests were conducted on the PA66/$CaCl_2$ composites at 230, 235, and 240 °C, in which the results are shown in Figures S1, S2, and S3. As seen in Figure S1a, the B0 sample exhibits a relatively sharp single crystallization peak when the isothermal crystallization temperature is 230 °C, with the crystallization time at the maximum crystallization rate being 5.94 min, completing crystallization in a short time. After adding 1 wt %

**Table 2. DSC Results for PA66/$CaCl_2$ Composites**

| | cooling | | second heating | | |
|---|---|---|---|---|---|
| samples | $T_c$ (°C) | $\Delta H_c$ (J $g^{-1}$) | $T_m$ (°C) | $\Delta H_m$ (J $g^{-1}$) | crystallinity (%) |
| B0 | 233.2 | 62.3 | 260.4 | 76.1 | 40.4 |
| B1 | 229.9 | 54.3 | 258.2 | 69.7 | 37.0 |
| B3 | 220.1 | 53.0 | 252.6 | 59.6 | 31.7 |
| B5 | 217.0 | 50.3 | 251.1 | 57.9 | 30.8 |

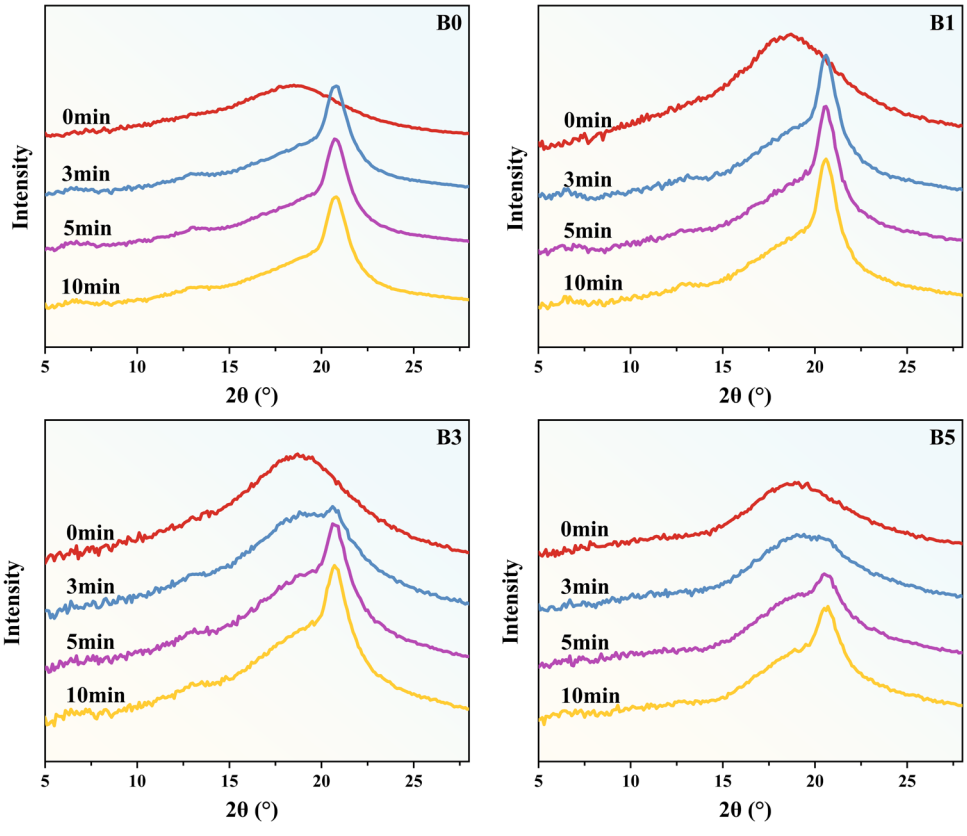


**Figure 3.** WAXS curves of PA66 and its composites under isothermal crystallization behavior at 250 °C.



https://doi.org/10.1021/acsomega.4c11028
ACS Omega 2025, 10, 19444−19452

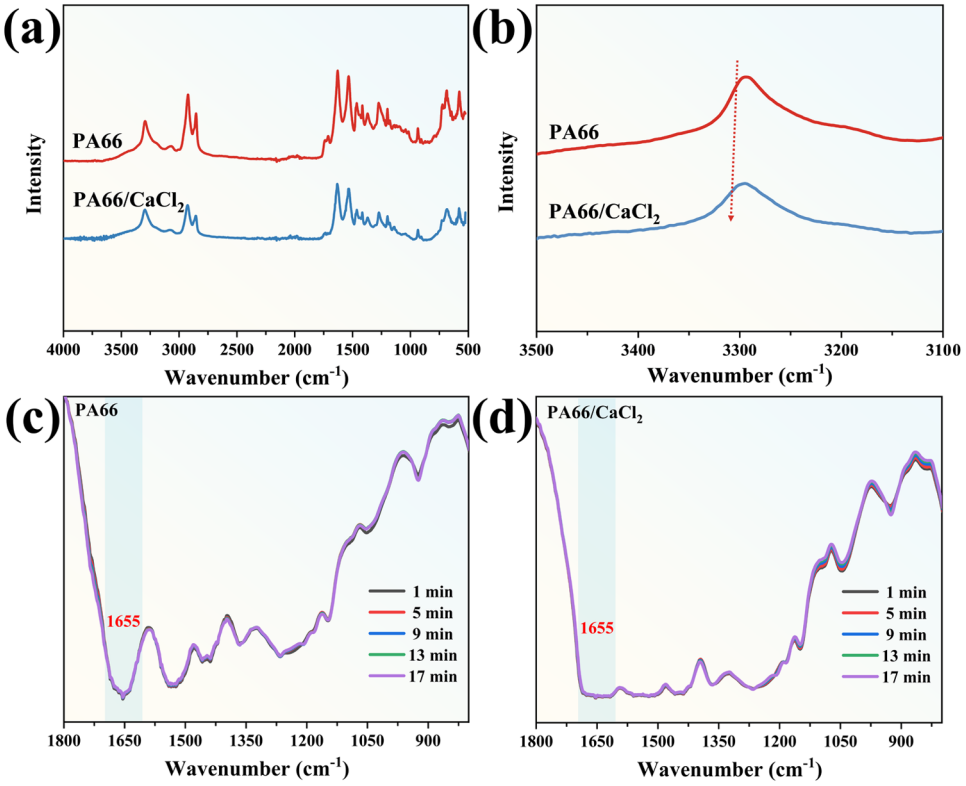


**Figure 4.** FTIR (a, b) and isothermal FTIR (c,d) of PA66 and PA66/$CaCl_2$.

$CaCl_2$, the onset time of crystallization in B1 is slightly delayed, but it still shows a sharp single crystallization peak, with the crystallization time at the maximum rate extending to 6.20 min. With further increases in the $CaCl_2$ content, samples B3 and B5 display broader and more gradual crystallization peaks, and the crystallization time at the maximum rate also significantly extends. This also verifies that the addition of $CaCl_2$ reduces the crystallization rate of PA66. When the isothermal crystallization temperature is increased to 240 °C, the crystallization time trends for different samples are similar to those at 230 °C. Notably, for samples B3 and B5, the crystallization peaks are barely observable, indicating a substantial decrease in crystallization ability (Figure S3a). During the subsequent heating process after 24 min of isothermal crystallization, the crystallinity of PA66 samples with $CaCl_2$ is significantly lower than that of pure PA66. The higher the $CaCl_2$ content, the lower the crystallinity. In particular, there is no melting peak during the subsequent heating process (Figure S3b) for the B5 sample, further confirming that the addition of $CaCl_2$ has a significant inhibitory effect on PA66 crystallization, as shown in Tables S1, S2, and S3.

**3.2. Crystalline Morphology Studies of PA66/$CaCl_2$ Composites.** The morphology and the crystallinity of pure PA66 and PA66/$CaCl_2$ composites as a function of time were carried out by POM and WAXS. All the samples were melted followed by a rapid cooling process to 245, 250, and 255 °C. The appearance of spherulites among the samples differs, indicating that the crystallization degrees of the samples vary under the same isothermal crystallization time. Due to the rapid crystallization ability of pure PA66, B0 forms a large number of small spherulites merely after 1 min of isothermal crystallization at 250 °C (Figure S5). For B1, B3, and B5 samples, small crystallites can be observed after 3, 5, and 20 min, respectively, suggesting that the crystallization rate gradually decreases with the increases in $CaCl_2$ content. At a higher temperature (255 °C, Figure S6), the appearance of crystals was slightly delayed and showed at 3, 10, and 20 min for B0, B1, and B3 samples, respectively. The reduced crystallization rate can also be observed at 245 °C (Figure S4). Consistent with the isothermal crystallization behavior in DSC, these results further confirmed the inhibition effect of $CaCl_2$ on the crystallization of PA66 composites.

The corresponding WAXS curves of PA66/$CaCl_2$ blends at 250 °C are shown in Figure 3 and Figure S7. No crystallization peaks were detected in the B0 samples, indicating an amorphous state. After 3 min of isothermal crystallization, B0 and B1 samples exhibited distinct diffraction peaks at $2\theta \approx 20.5°$, corresponding to the $\alpha$-phase crystal.[34] As the isothermal time increased, the diffraction peaks slightly narrowed and the crystallinity gradually increased. When the $CaCl_2$ content increased to 3 and 5 wt %, weak crystallization peaks appeared after 3 and 5 min of isothermal crystallization, respectively, indicating that the addition of $CaCl_2$ reduces the crystallization rate of PA66. This result is consistent with the POM results mentioned earlier, both indicating that the crystallization rate of PA66/$CaCl_2$ blends decreases significantly compared to that of pure PA66. These findings demonstrate that $CaCl_2$ effectively regulates the crystallization behavior of PA66.

**3.3. FTIR Studies toward the Interaction between PA66 and $CaCl_2$.** By comparison with the FTIR spectrum of pure PA66, variations are found in amide bands in PA66/$CaCl_2$ systems. FTIR and isothermal FTIR to study the crystalline polymer materials are reported in the previous work such as for PA6, PA66, and PLA.[20,31,35−37] The bands at about


https://doi.org/10.1021/acsomega.4c11028
ACS Omega 2025, 10, 19444−19452

3300 and 1640 $cm^{-1}$ can be assigned to N−H and C═ O stretching vibration bonds, respectively, strongly depending on hydrogen bonding interactions between the PA66 chains.[38] The amide band at 3293 $cm^{-1}$ for pure PA66 in Figure 4 is characteristic of hydrogen-bonded polyamides in a crystalline region. However, this peak exhibited a blueshift with the peak moving toward higher frequency (3 $cm^{-1}$). This phenomenon showed that the hydrogen bonds between N−H and C═O are weakened. This was because the coordination between amide groups from PA66 and $Ca^{2+}$and the free N−H bonds was produced, which also has been reported previously in nylon-metal systems. The amide group as a potentially bifunctional electron donor (a 2 $sp^2$ "lone pair" at the oxygen atom and a $2p_z^2$ "lone pair" at a nitrogen atom). Overlap of $2p_z$ orbitals of the atoms within the planar amide group would reduce the electron density on the nitrogen atom. Therefore, the strong electron-withdrawing effect of $Ca^{2+}$ on the oxygen atom of the carbonyl group is shown (Figure 5).[22,39,40]

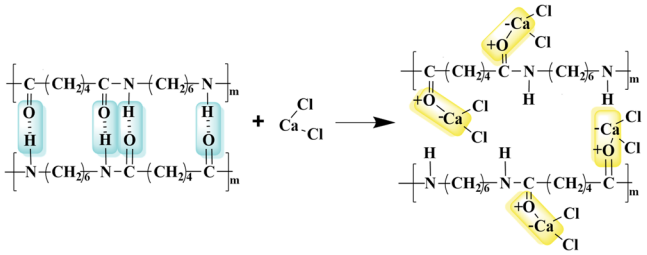

**Figure 5.** Mechanism scheme of the coordination effect between $CaCl_2$ and amine groups.

Dramatically different spectrum behaviors are observed in isothermal FTIR at 250 °C. As shown in Figure 4c,d, the intensity of the peak located at 1655 $cm^{-1}$ is reduced, further indicating the reduction of C═O bands resulted from electron-withdrawing effects. Therefore, inhibition of the hydrogen bonds resulting from the coordination between PA66 and metal salt led to a slowed down crystallization rate and crystallinity (Figure 5). This explained the crystallization behavior in POM, WAXS, and DSC.

**3.4. Fabrication of PA66/$CaCl_2$ Fiber and Its Property Study.** The rheological property is crucial to the spinnability of polymer composites during the melt spinning process. Therefore, the viscosity of a series of PA66/$CaCl_2$ composites is shown in Figure 6. At 280 °C, the shear viscosity of each sample gradually decreases as the shear rate increases. At the same shear rate, the shear viscosity of the samples ranks from highest to lowest as B5 > B3 > B1 > B0, indicating that compared to pure PA66, the friction between the molecules in the PA66/$CaCl_2$ composites is enhanced. The increase in the viscosity may decrease the fluidity of the polymer melt upon the spinning process. Additionally, the shear viscosity further increases with the rise in $CaCl_2$ content. This may be attributed to the coordination between calcium ions and the carbonyl groups in PA66, forming a complex. The complex acts as a connector, increasing the friction between molecular chains and inhibiting the disentanglement behavior of the molecular chains under shear force, thus causing the increase in melt viscosity of the PA66/$CaCl_2$ blend as the addition of $CaCl_2$ increases. However, the extremely high viscosity, on the contrary, may deteriorate the spinnability of PA66.

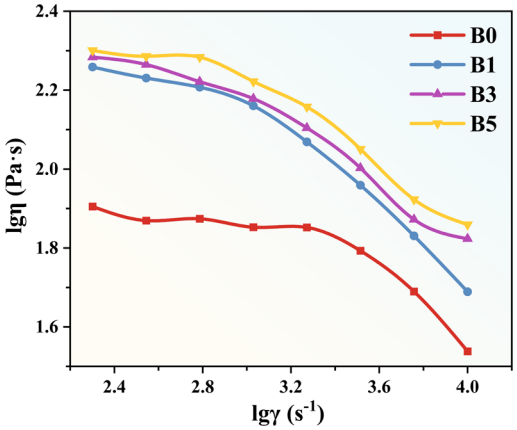


**Figure 6.** Shear viscosity of PA66/$CaCl_2$ composites as a function of shear rate under 280 °C.

Based on the rheological property of PA66 composites, the loading of $CaCl_2$ was reduced between 0.5 and 3 wt % to achieve PA66 composites with moderate viscosity, which facilitate the melt spinning process. The spinnability and fabrication of nascent fibers were first explored under 280 °C. The produced B0-F and B0.5-F nascent fibers tended to break easily during the drawing process and could not be drawn successfully. The B1-F drawn fiber can be prepared at a draw ratio of 3.5, indicating that the addition of $CaCl_2$ improves the spinnability of PA66. This may be attributed to the regulation of PA66's crystallization performance during the spinning process. This can be verified by the crystalline state of PA66/$CaCl_2$ nascent fibers via DSC and WAXS as shown in Figure 7. As the research aimed to evaluate how $CaCl_2$ influences the actual crystallinity developed during the melt spinning process, the first heating curve directly reflects the as-spun fiber's crystalline state prior to any thermal history reset. From Figure 7a, it can be observed that B0-F exhibits a sharp crystallization melting peak at 250 °C, while both B0.5-F and B1-F nascent fibers show a cold crystallization peak in addition to the melting endothermic peak. As the $CaCl_2$ content increases from 0.5 to 1 wt %, the cold crystallization peak of B1-F nascent fibers becomes more pronounced, indicating that the crystallinity of PA66 nascent fibers containing $CaCl_2$ is lower, and crystallization occurs during the heating process. The corresponding 1D WAXS curves are shown in Figure 7b. The diffraction peak intensity of B0.5-F and B1-F nascent fibers decreases compared with that of B0-F fibers, suggesting that the addition of $CaCl_2$ inhibits the crystallinity of PA66 nascent fibers, thereby providing favorable conditions for subsequent drawing. The crystallinity gradually decreased to 38.7, 35.7, and 33.9% (Table 3). The 2D WAXS diffraction patterns and orientation degrees of different fibers are shown in Figure 7c,d. From Figure 7d, it can be observed that the orientation degree of the nascent fibers decreases progressively with the increase in $CaCl_2$ content, with orientation factors of 0.080, 0.073, and 0.053. As the orientation degree decreases, the oriented arrangement of segments in PA66 is reduced, increasing the number of movable segments, which is beneficial for subsequent drawing.

The mechanical property data for each nascent fiber are shown in Table 4. As the $CaCl_2$ content increases, the elongation at break of the nascent fibers improves from 207.26 to 255.38%. During the drawing process of B1-F nascent fibers, the formation of hydrogen bonds is inhibited, preventing


https://doi.org/10.1021/acsomega.4c11028
ACS Omega 2025, 10, 19444−19452

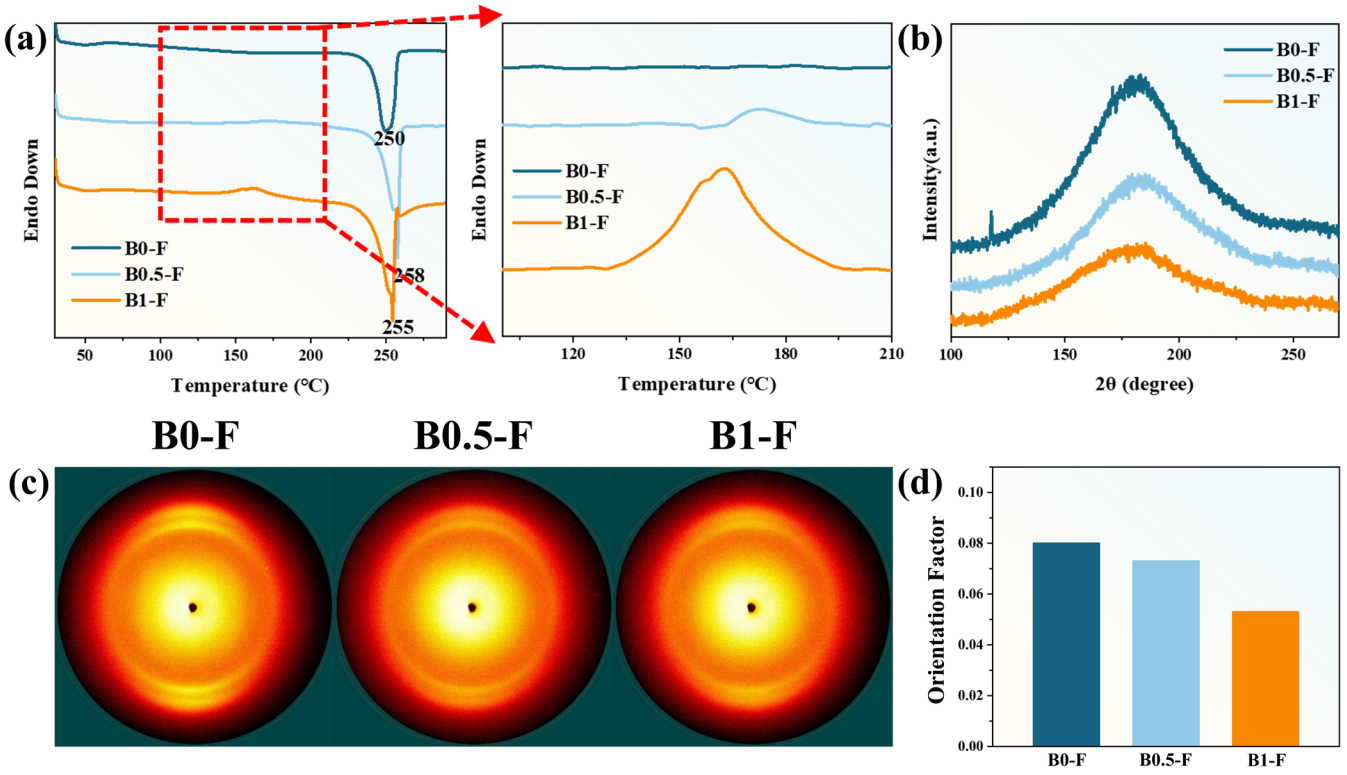


**Figure 7.** Crystallization behavior of PA66/$CaCl_2$ as-spun fiber: (a) first heating curve in DSC, (b) WAXS curve, (c) 2D WAXS diffraction patterns, and (d) orientation factor.

**Table 3. Properties of PA66/$CaCl_2$ Blend Fibers**

| as-spun fiber | composition of PA66 (%) | composition of $CaCl_2$ (%) | spinnability | draw ratio | crystallinity (%) | orientation factor |
|---|---|---|---|---|---|---|
| B0-F | 100.0 | 0 | + | | 38.7 | 0.080 |
| B0.5-F | 99.5 | 0.5 | ++ | | 35.7 | 0.073 |
| B1-F | 99.0 | 1.0 | +++ | 3.5 | 33.9 | 0.053 |
| B3-F | 97.0 | 3.0 | | | | |

**Table 4. Mechanical Property of Nascent Fiber and Drawn Fibers**

| samples | denier (dtex) | breaking strength (cN/dtex) | elongation at break (%) |
|---|---|---|---|
| B0-F | 127 | 1.37 | 207.26 |
| B0.5-F | 160 | 1.15 | 250.56 |
| B1-F | 163 | 1.22 | 255.38 |
| B1-F' | 49 | 5.16 | 16.13 |

crystallization and thereby increasing the orientation degree. Therefore, the orientation degree of the drawn B1-F' fiber increases significantly, with the corresponding orientation factor rising to 0.133 (Figure S8). The improved orientation degree is favorable for enhancing the mechanical properties of the fiber. In the subsequent drawing stage, directional forces are applied, promoting the orientation of the nascent fibers and resulting in highly oriented drawn fibers. After drawing and heat setting, the breaking strength of the B1-F' fiber significantly increases, reaching 5.16 cN/dtex. These results indicate that the addition of $CaCl_2$ can regulate the crystallization rate of PA66, enhancing its drawability and providing insights for the development of fine denier, high-performance PA66 fibers.

## 4. CONCLUSIONS

In summary, $CaCl_2$ as a crystallization regulator improved spinnability and drawability of PA66. The coordination interaction between $Ca^{2+}$ and amine groups, which exhibited a redshift in FTIR, weakened the original hydrogen bonds and decreased the crystallization rate. The PA66 drawn fiber containing 1 wt % $CaCl_2$ was successfully prepared via melt spinning with the draw ratio at 3.5. The mechanical strength and elongation at break of the as-prepared PA66 fiber improved to 5.16 cN/dtex and 16.13%, respectively.

## ■ ASSOCIATED CONTENT

### Supporting Information

The Supporting Information is available free of charge at https://pubs.acs.org/doi/10.1021/acsomega.4c11028.

Three tables and eight figures related to experimental results covering crystallization behavior of PA66 composites and their fiber (PDF)

## ■ AUTHOR INFORMATION

### Corresponding Author

**Xiuqin Zhang** − *Beijing Key Laboratory of Clothing Materials R & D and Assessment, Beijing Engineering Research Center of Textile Nanofiber and School of Materials Design &*



https://doi.org/10.1021/acsomega.4c11028
*ACS Omega* 2025, 10, 19444−19452

*Engineering, Beijing Institute of Fashion Technology, Beijing 100029, China;* orcid.org/0000-0002-8687-4280; Email: clyzxq@bift.edu.cn

### Authors

**Jianing Wang** − *School of Materials Design & Engineering, Beijing Institute of Fashion Technology, Beijing 100029, China*

**Jing Zhang** − *School of Materials Design & Engineering and Beijing Key Laboratory of Clothing Materials R & D and Assessment, Beijing Engineering Research Center of Textile Nanofiber, Beijing Institute of Fashion Technology, Beijing 100029, China;* orcid.org/0000-0002-1516-3019

**Yanlong Zhu** − *School of Materials Design & Engineering, Beijing Institute of Fashion Technology, Beijing 100029, China;* orcid.org/0000-0003-1213-8819

**Shuo Yang** − *School of Materials Design & Engineering, Beijing Institute of Fashion Technology, Beijing 100029, China*

**Zhenfeng Dong** − *School of Materials Design & Engineering and Beijing Key Laboratory of Clothing Materials R & D and Assessment, Beijing Engineering Research Center of Textile Nanofiber, Beijing Institute of Fashion Technology, Beijing 100029, China*

**Rui Wang** − *School of Materials Design & Engineering and Beijing Key Laboratory of Clothing Materials R & D and Assessment, Beijing Engineering Research Center of Textile Nanofiber, Beijing Institute of Fashion Technology, Beijing 100029, China;* orcid.org/0000-0001-5886-3261

Complete contact information is available at: https://pubs.acs.org/10.1021/acsomega.4c11028

### Notes

The authors declare no competing financial interest.

## ■ ACKNOWLEDGMENTS

We acknowledge the financial support from the National Key Program of China (No. 2022-1400602).

## ■ REFERENCES

(1) Kisner, A.; Rainert, K. T.; Ferrari, F.; Nau, C. T.; Barcellos, I. O.; Pezzin, S. H.; Andreaus, J.; et al. Chemical functionalization of polyamide 6.6 fabrics. *React. Funct. Polym.* **2013**, *73*, 1349−1356.

(2) Huang, X. H.; Li, B.; Shi, B. L.; et al. Investigation on interfacial interaction of flame retarded and glass fiber reinforced PA66 composites by IGC/DSC/SEM. *J. Polymer.* **2008**, *49*, 1049−1055.

(3) Li, L. P.; Li, B.; Tang, F. Influence of maleic anhydride-grafted EPDM and flame retardant on interfacial interaction of glass fiber reinforced PA-66. *J. Eur. Polym.* **2007**, *43*, 2604−2611.

(4) Lin, D. J.; Chang, C. L.; Lee, C. K.; et al. Fine structure and crystallinity of porous Nylon 66 membranes prepared by phase inversion in the water/formic acid/Nylon 66 system. *J. Eur. Polym.* **2006**, *42*, 356−367.

(5) Albano, C.; Sciamanna, R.; Gonzalez, R.; et al. Analysis of nylon 66 solidification process. *J. Eur. Polym.* **2001**, *37*, 851−860.

(6) Wang, Y. J. Fiber and Textile Waste Utilization. *J. Waste Biomass Valorization* **2010**, *1*, 135−143.

(7) Bedia, E. L.; Tsuji, M.; Tosaka, M.; et al. Morphologies of melt-crystallized thin films of Nylon-6, Nylon-6,6, and their blends as revealed by transmission electron microscopy. *J. Macromol. Sci. Phys.* **2001**, *40*, 1079−1096.

(8) Suzuki, A.; Endo, A. Preparation of high modulus nylon 46 fibres by high-temperature zone-drawing. *Polymer* **1997**, *38*, 3085−3089.

(9) Pennings, A. J.; Smook, J.; de Boer, J.; et al. Process of preparation and properties of ultra-high strength polyethylene fibers. *Pure Appl. Chem.* **1983**, *55*, 777−798.

(10) Smith, P.; Lemstra, P. J. Ultra-high-strength polyethylene filaments by solution spinning/drawing. *J. Journal of Materials Science.* **1980**, *15*, 505−514.

(11) Shi, C. M.; Zhao, G. L.; Jia, Q. X.; et al. Research progress in complex modification of polyamide. *J. China Synth. Fiber Ind.* **2010**, *33*, 47−51.

(12) Arimoto, H.; Ishibashi, M.; Hirai, M.; et al. Crystal structure of the γ-form of nylon 6. *J. Journal of Polymer Science Part A: General Papers* **1965**, *3*, 317−326.

(13) Zachariades, A. E.; Porter, R. S. Reversible plasticization of nylons 6 and 11 with anhydrous ammonia and their deformation by solid-state coextrusion. *J. Appl. Polym. Sci.* **1979**, *24*, 1371−1382.

(14) Zhang, Y. M.; Ye, Y. T.; Wang, H. P. In-situ Polymerization of Rare-Earth Luminous PA6. *J. Macromol. Symp.* **2004**, *216*, 1−8.

(15) Ciferri, A.; Bianchi, E.; Marchese, F.; et al. Differential scanning calorimetry of poly(caproamide)/inorganic salt systems. *J. Die Makromolekulare Chemie.* **1971**, *150*, 265−270.

(16) Valenti, B.; Bianchi, E.; Greppi, G.; et al. Bulk properties of synthetic polymer-inorganic salt systems. Melting behavior of salted poly(caproamide). *J. The Journal of Physical Chemistry* **1973**, *77*, 389−395.

(17) Richardson, A.; Ward, I. M. Production and properties of fibers spun from nylon 6/lithium chloride mixtures. *J. Journal of Polymer Science: Polymer Physics Edition.* **1981**, *19*, 1549−1565.

(18) Acierno, D.; Bianchi, E.; Ciferri, A.; et al. Bulk properties of synthetic polymer-inorganic salt systems. III. Flow behavior and glass transition of salted polycaproamide. *J. Polym. Sci., Polym. Symp.* **1976**, *54*, 259−269.

(19) Acierno, D.; La Mantia, F. P.; Polizzotti, G.; et al. Bulk properties of synthetic polymer-inorganic salt systems. V. Mechanical properties of oriented poly(caproamide). *J. Polym. Sci. B Polym. Phys.* **1979**, *17*, 1903−1912.

(20) Liu, S. X.; Zhang, C. F.; Liu, Y. H.; et al. Coordination between yttrium ions and amide groups of polyamide 6 and the crystalline behavior of polyamide 6/yttrium composites. *J. Mol. Struct.* **2012**, *1021*, 63−69.

(21) Niu, X. L.; Zhao, L. Q.; Yin, M.; et al. Mineralized Polyamide66/Calcium Chloride Nanofibers for Bone Tissue Engineering, Tissue Eng. Part C. *Methods* **2020**, *26*, 352−363.

(22) Rietzler, B.; Bechtold, T.; Pham, T. Controlled Surface Modification of Polyamide 6.6 Fibres Using $CaCl_2/H_2O/EtOH$ Solutions. *Polymers* **2018**, *10*, 207.

(23) Rietzler, B.; Bechtold, T.; Pham, T. Spatial Structure Investigation of Porous Shell Layer Formed by Swelling of PA66 Fibers in $CaCl_2/H_2O/EtOH$ Mixtures. *Langmuir* **2019**, *35*, 4902−4908.

(24) Yin, Y. Y. The study on spinning of ultra high molecular polyamide-6, D. *Beijing Inst. Fashion Technol.* **2009**, 58−59.

(25) Seo, J.; Takahashi, H.; Nazari, B.; et al. Isothermal Flow-Induced Crystallization of Polyamide 66 Melts. *Macromolecules* **2018**, *51*, 4269−4279.

(26) Won, J. C.; Fulchiron, R.; Douillard, A.; et al. Effect of the pressure on the crystallization behavior of polyamide 66. *J. Appl. Polym. Sci.* **2001**, *80*, 1021−1029.

(27) Rhoades, A. M.; Williams, J. L.; Androsch, R. Crystallization kinetics of polyamide 66 at processing-relevant cooling conditions and high supercooling. *J. Thermochim. Acta* **2015**, *603*, 103−109.

(28) Zhang, S. Y.; Ma, J. H. Tailored Process for Spinning Fine Denier Bio-Based Polyamide 56 Fibers. *J. Biobased Mater. Bioenergy* **2019**, *13*, 102−108.

(29) Zhang, C. F.; Liu, Y. H.; Liu, S. X.; et al. Crystalline behaviors and phase transition during the manufacture of fine denier PA6 fibers. *J. Sci. China Chem.* **2009**, *52*, 1835−1842.

(30) Zhang, X. S.; Buzinkai, J.; Quinn, E.; et al. Key Insights into the Differences between Bimodal Crystallization Kinetics of Polyamide 66 and Polyamide 6. *Macromolecules* **2022**, *55*, 9220−9231.

(31) Vasanthan, N.; Ruetsch, S. B.; Salem, D. R. Structure development of polyamide-66 fibers during drawing and their microstructure characterization. *J. Polym. Sci., Polym. Phys.* **2002**, *40*, 1940−1948.
(32) Chi, E. Y.; An, M. F.; Yao, G. B.; et al. The Influence of Epitaxial Crystallization on the Mechanical Properties of Polyamide 66/Reduced Graphene Oxide Nanocomposite Injection Bar. *J. Crystals* **2017**, *7*, 384.
(33) Yang, B.; Li, Q.; Li, X. L.; et al. Influence of nucleating agent on crystallization behavior ofL-polylatic acid/D-polylatic acid. *New Chem. Mater.* **2019**, *47*, 188−192.
(34) Sengupta, R.; Ganguly, A.; Sabharwal, S.; et al. MWCNT reinforced Polyamide-6,6 films: preparation, characterization and properties. *J. Mater. Sci.* **2007**, *42*, 923−934.
(35) Ma, Y.; Zhou, T.; Su, G.; Li, Y.; Zhang, A.; et al. Understanding the crystallization behavior of polyamide 6/polyamide 66 alloys from the perspective of hydrogen bonds: projection moving-window 2D correlation FTIR spectroscopy and the enthalpy. *RSC Adv.* **2016**, *6*, 87405−87415.
(36) Porubská, M.; Szöllős, O.; Kóňová, A.; et al. FTIR spectroscopy study of polyamide-6 irradiated by electron and proton beams. *J. Polymer Degradation and Stability* **2012**, *97*, 523−531.
(37) Zhuo, R. R.; Zhang, Y. Y.; Li, G. L.; et al. Structural evolution of poly(lactic acid) upon uniaxial stretching investigated by in situ infrared spectroscopy. *J. Vibrational Spectroscopy* **2016**, *86*, 262−269.
(38) Vasanthan, N.; Kotek, R.; Jung, D. W.; et al. Lewis acid−base complexation of polyamide 66 to control hydrogen bonding, extensibility and crystallinity. *J. Polymer.* **2004**, *45*, 4077−4085.
(39) Roberts, M. F.; Jenekhe, S. A. Lewis acid complexation of polymers: gallium chloride complex of nylon 6. *J. Chemistry of Materials* **1990**, *2*, 224−226.
(40) Roberts, M. F.; Jenekhe, S. A. Site-specific reversible scission of hydrogen bonds in polymers: an investigation of polyamides and their Lewis acid-base complexes by infrared spectroscopy. *J. Macromolecules* **1991**, *24*, 3142−3146.


https://doi.org/10.1021/acsomega.4c11028
*ACS Omega* 2025, 10, 19444−19452